# Supporting Information for

# The Critical Role of nπ* States in the Photophysics and Thermally Activated Delayed Fluorescence of Spiro Acridine-Anthracenone

**AUTHORS**

Larissa Gomes Franca, Yun Long, Chunyong Li, Andrew Danos, and Andrew Monkman*

OEM Research group, Department of Physics, Durham University, South Road, Durham, DH1 3LE, United Kingdom.

## Experimental Details

### Sample Preparation

Solutions of ACRSA for photophysical characterization were prepared at low concentration of 50 μM for some measurements to strictly prevent intermolecular interactions, or at high concentration of 1 mg/mL for other measurements to give improved signal to noise. ACRSA was dissolved in solvents MCH, toluene, and DCM, which have varying polarities. Solutions were left to stir overnight with the use of a magnetic stirrer bar at varying temperatures. For measurements in oxygen free conditions, solutions were degassed by 5 freeze-thaw cycles in appropriate degassing cuvettes. For film measurements, films were drop cast from mixed toluene solutions of ACRSA and Zeonex, and deposited onto a preheated quartz or sapphire substrate (70°C) and allowed to dry thoroughly (~3 minutes). For transient absorption measurements, an ACRSA stock solution was prepared by dissolving ACRSA in anhydrous toluene overnight at 60 °C in a nitrogen glovebox. The solution was then transferred to a sealable 1 mm cuvette inside the glovebox, and removed for measurements.

### Photophysical Characterization

Absorption spectra for all solutions were collected using a double beam Shimadzu UV-3600 UV/VIS/NIR spectrophotometer. Steady state photoluminescence spectra were measured using both Jobin-Yvon Fluoromax-3 and Fluorolog spectrophotometers.

**Transient Absorption and Time-Resolved Photoluminescence**

Transient absorption measurements were carried out using a pump-probe spectroscopic setup. For measurements taking place within time interval 0-6 ns, the pump source took the form of a third harmonic generated using a Pharos amplified laser at 343 nm. For measurements spanning 0-1000 ns, an actinic YAG 355 nm laser (with pulse width 4 ns) was used as the pump source, whilst the probe beam was provided by a white light continuum ranging from 500-800 nm. Time-resolved photoluminescence spectra (including phosphorescence) and decays were measured using either a time-correlated single photon counting (TCSPC, Horiba Deltaflex) with a range of nanoled and laser diode excitation sources, or a nanosecond gated spectrograph-coupled iCCD (Stanford, 4Picos) and an Nd:YAG laser emitting at 355 nm (EKSPLA).

# Supporting Scheme

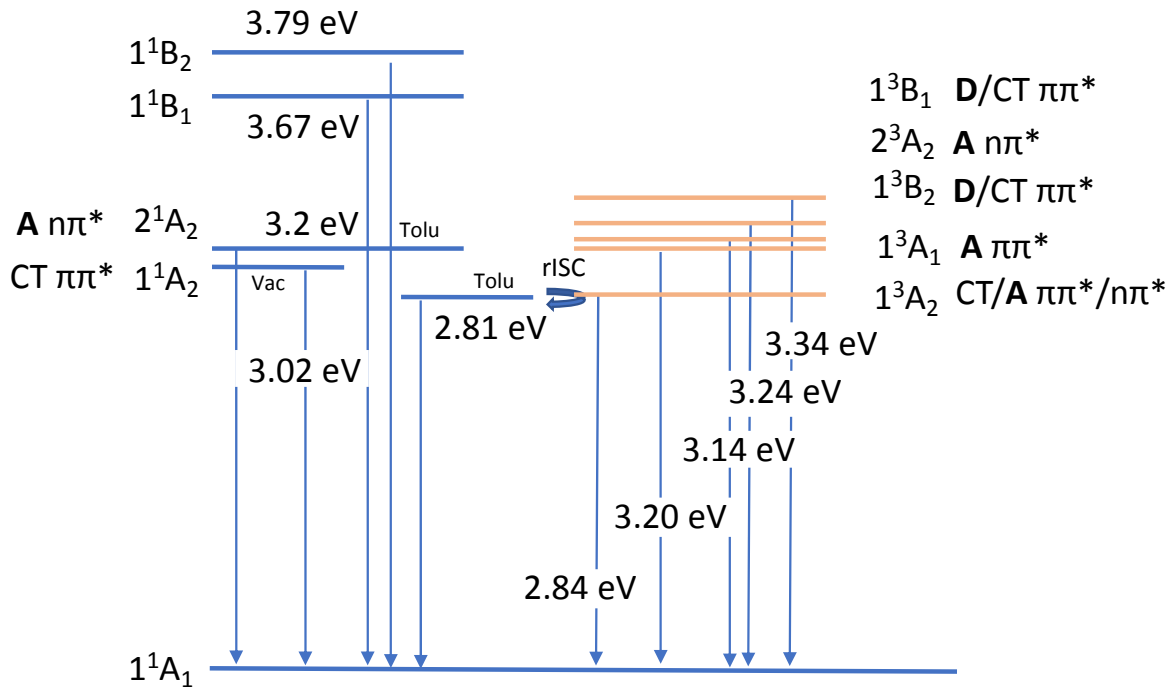


**Supporting Scheme 1:** State diagram composed from the calculated excited state characters and energies (nonadiabatic) of ACRSA in a toluene environment, after Lyskov and Marian.[1]

# Supporting Figures

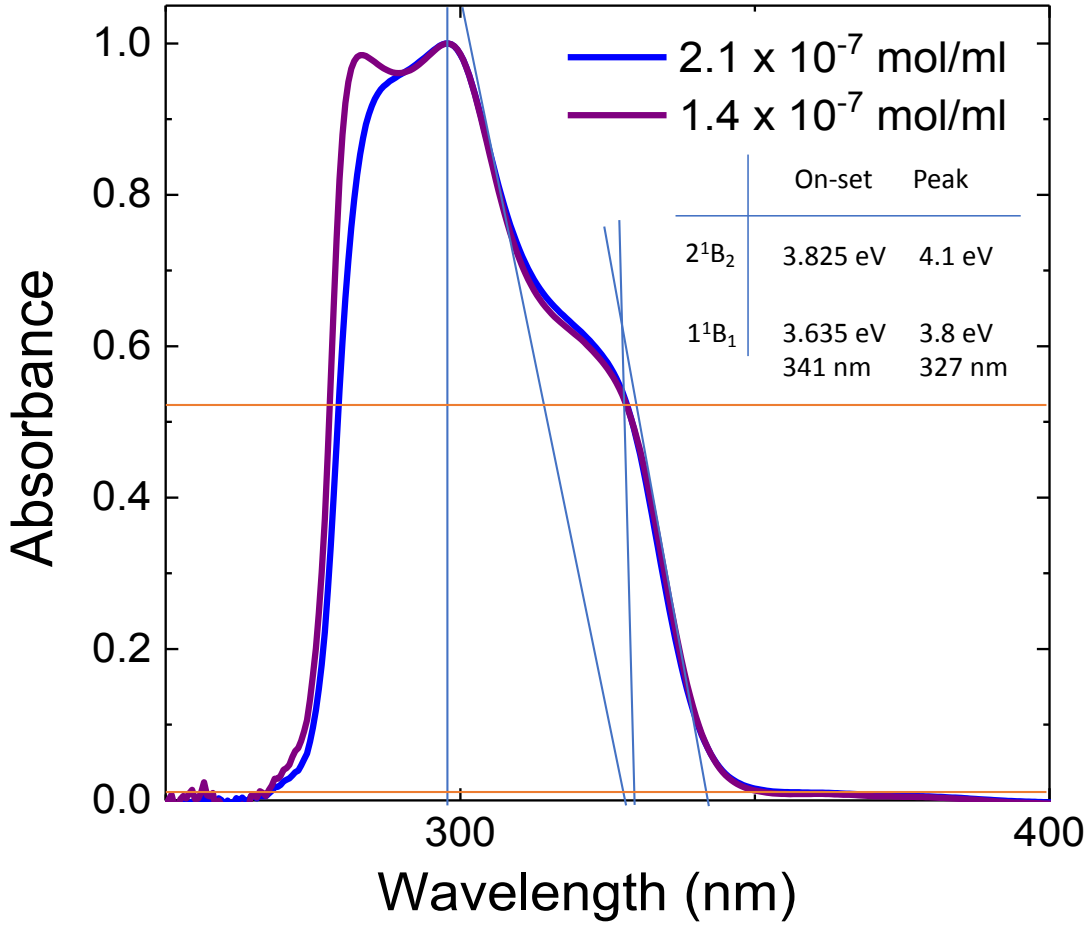


**Supporting Figure S1.** Absorption spectra of ACRSA in toluene at low concentrations. Peak and on-set energies of the two allowed excitonic transitions, $2^1B_2$ and $1^1B_1$ (following state labeling convention of Lyskov and Marian[1]) are given. The ratio of absolute absorbances at 330 nm/375nm is *ca*. 50.

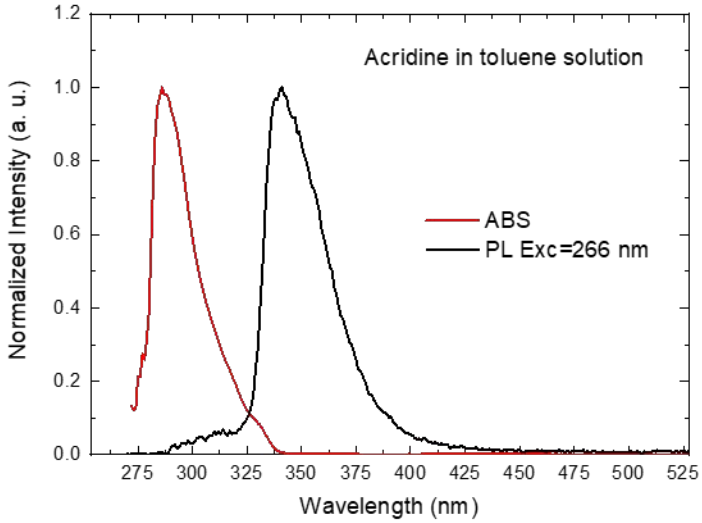


**Supporting Figure S2.** Normalized UV–vis absorption (red solid line) and PL spectra (black solid line) of acridine (donor unit) in toluene solution ($\lambda_{exc}$ = 266 nm). Data reported by dos Santos et al.[2]

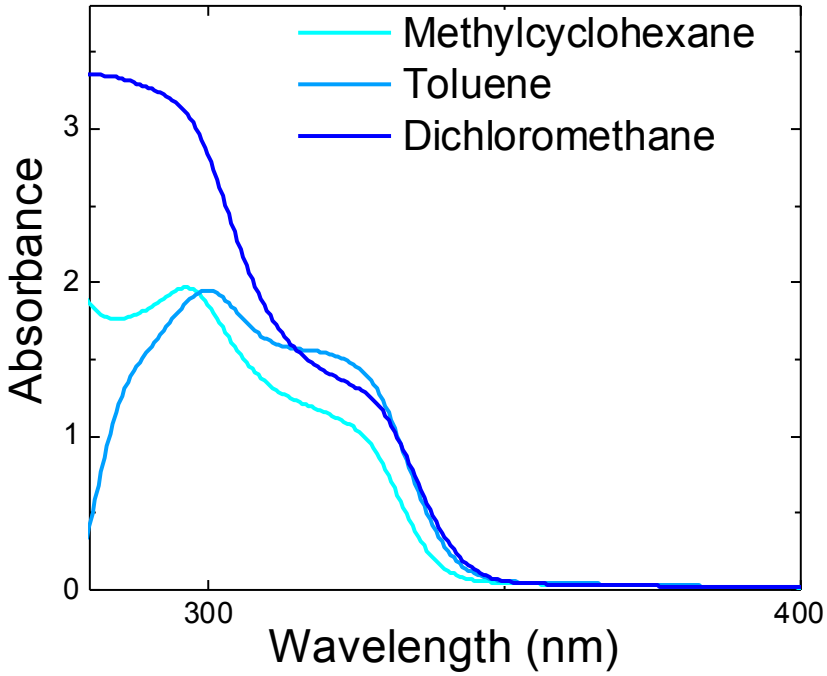


**Supporting Figure S3.** Absorbance measured in different solvents showing a small positive solvatochromic shift of the $2^1B_2$ and $1^1B_1$ transitions with increasing solvent polarity, indicative of strong π-π* transitions, but no new transitions.

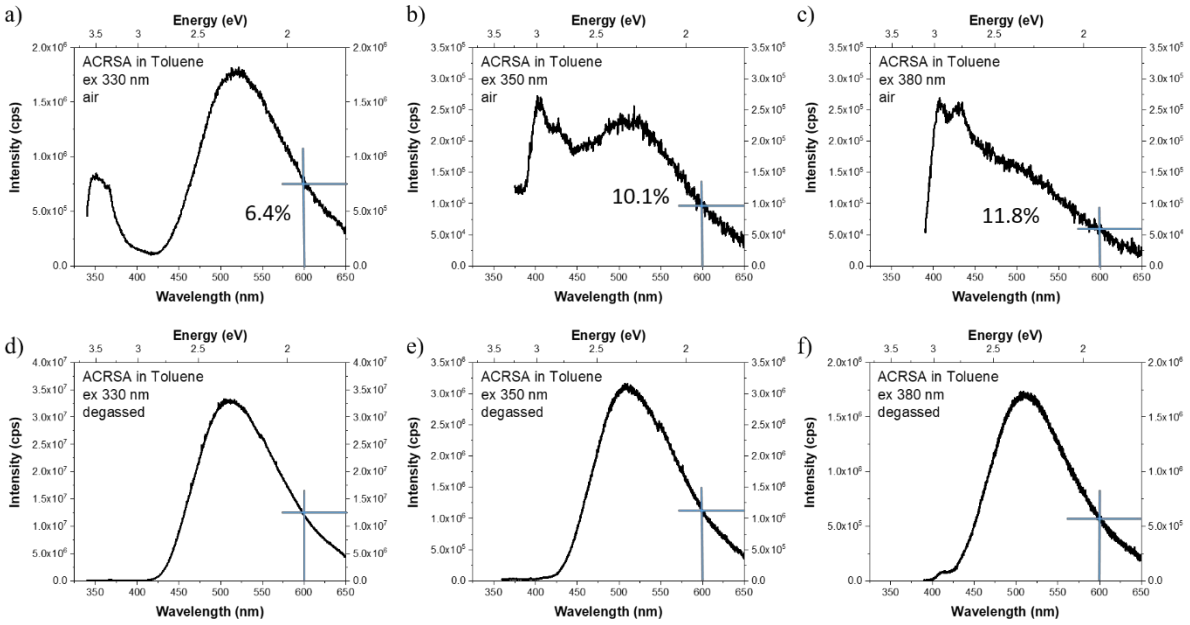


**Supporting Figure S4.** Emission spectra of ACRSA in toluene solution (50 μM) and the contribution of (charger transfer) delayed fluorescence calculated at 600 nm to avoid any contribution from local state emission. With direct excitation of the local and CT states (below 350 nm) we observe more prompt CT emission confirming the direct photo-production of both local and CT states at excitation wavelengths below 350 nm.

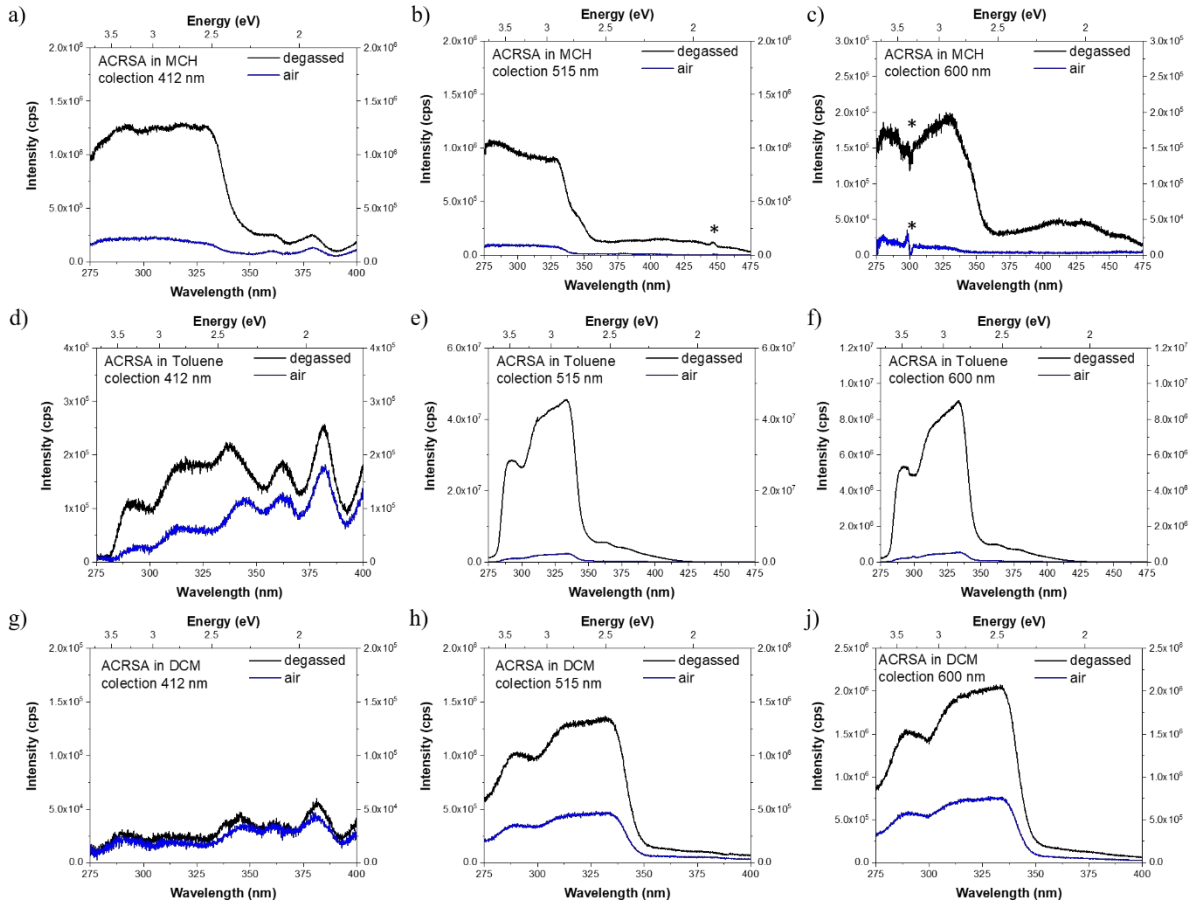


**Supporting Figure S5.** Excitation profiles from ACRSA in oxygenated and degassed MCH (top), toluene solution (middle panels) and DCM (bottom panels) (50 μM) recorded at emission wavelengths of 412 nm ($2^1A_2$ local state), 512 nm and 600 nm ($1^1A_2$ CT state). *Instrumental artefacts.

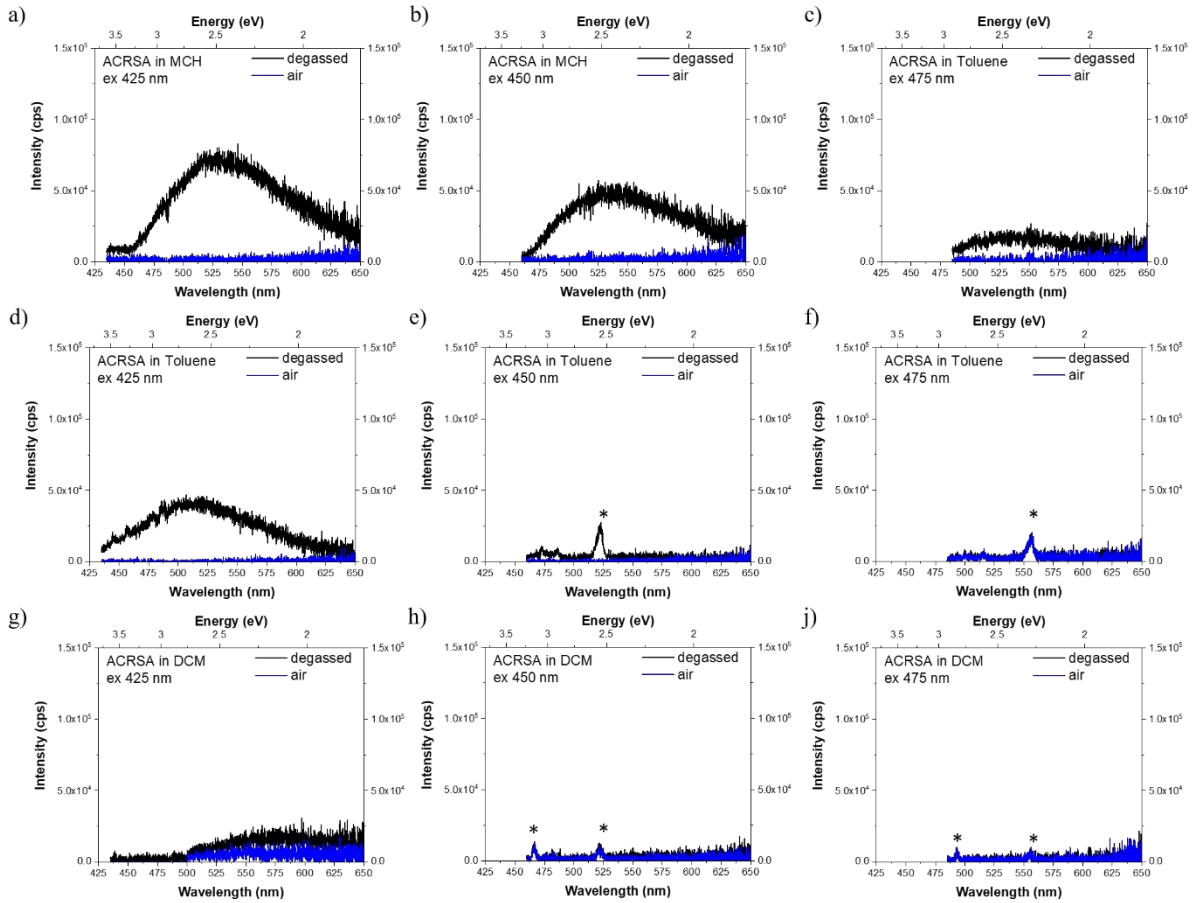


**Supporting Figure S6.** Comparison of emission spectra from ACRSA in MCH (a, b, c), toluene (d, e, f) and DCM (g, h, i) solutions excited deep in the tail of the absorption bands. By comparison we believe that in MCH where ACRSA is poorly soluble, the absorption below 425 nm comes from aggregate dimer species. In toluene and DCM, ACRSA has very good solubility and emission from these aggregate state are not seen. *Instrumental artefacts.

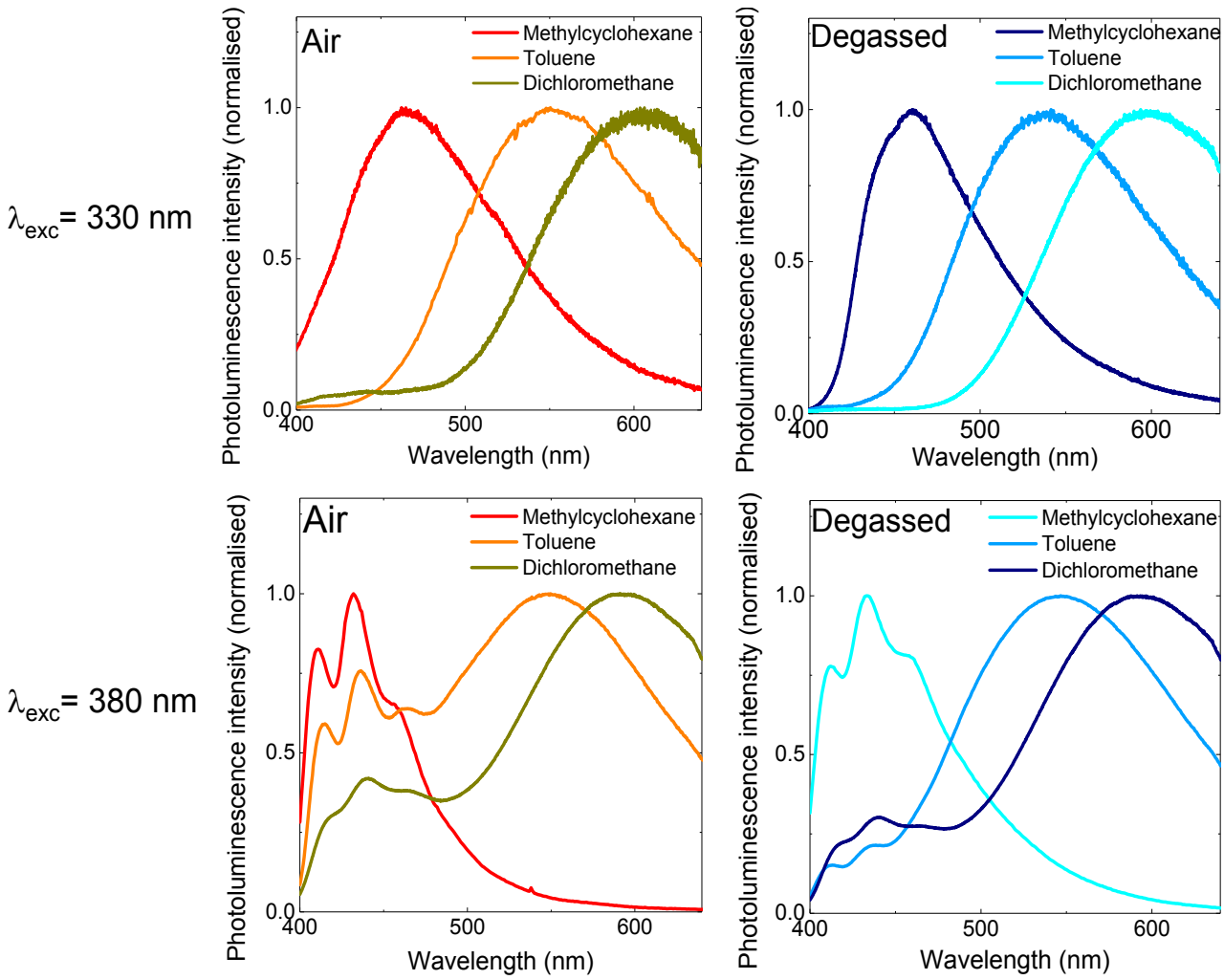


**Supporting Figure S7.** Emission spectra measured in aerated and deoxygenated ACRSA solutions dissolved in solvents of different polarities at concentration of 1 mg/mL, at excitation wavelengths $\lambda_{exc} =$ 330 nm and $\lambda_{exc} =$ 380 nm.

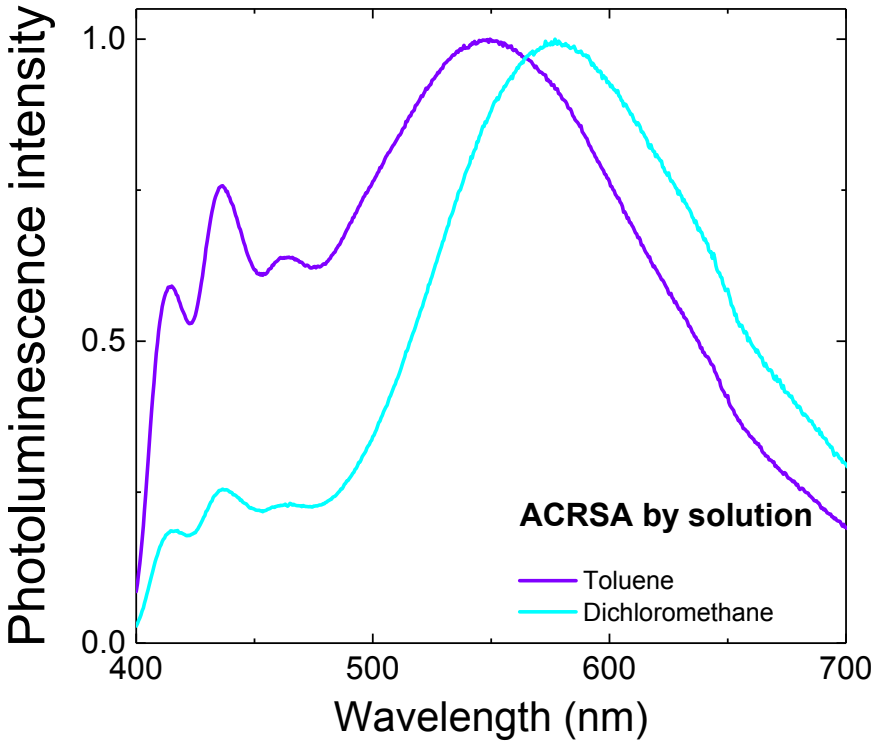


**Supporting Figure S8.** Emission spectra for ACRSA dissolved in Toluene and Dichloromethane (1 mg/mL) The local $2^1A_2$ transition is shown to be unaffected by polarity of the solvent even though it is calculated to be nπ* character, possibly due to its short lifetime and rapid quenching by ISC.

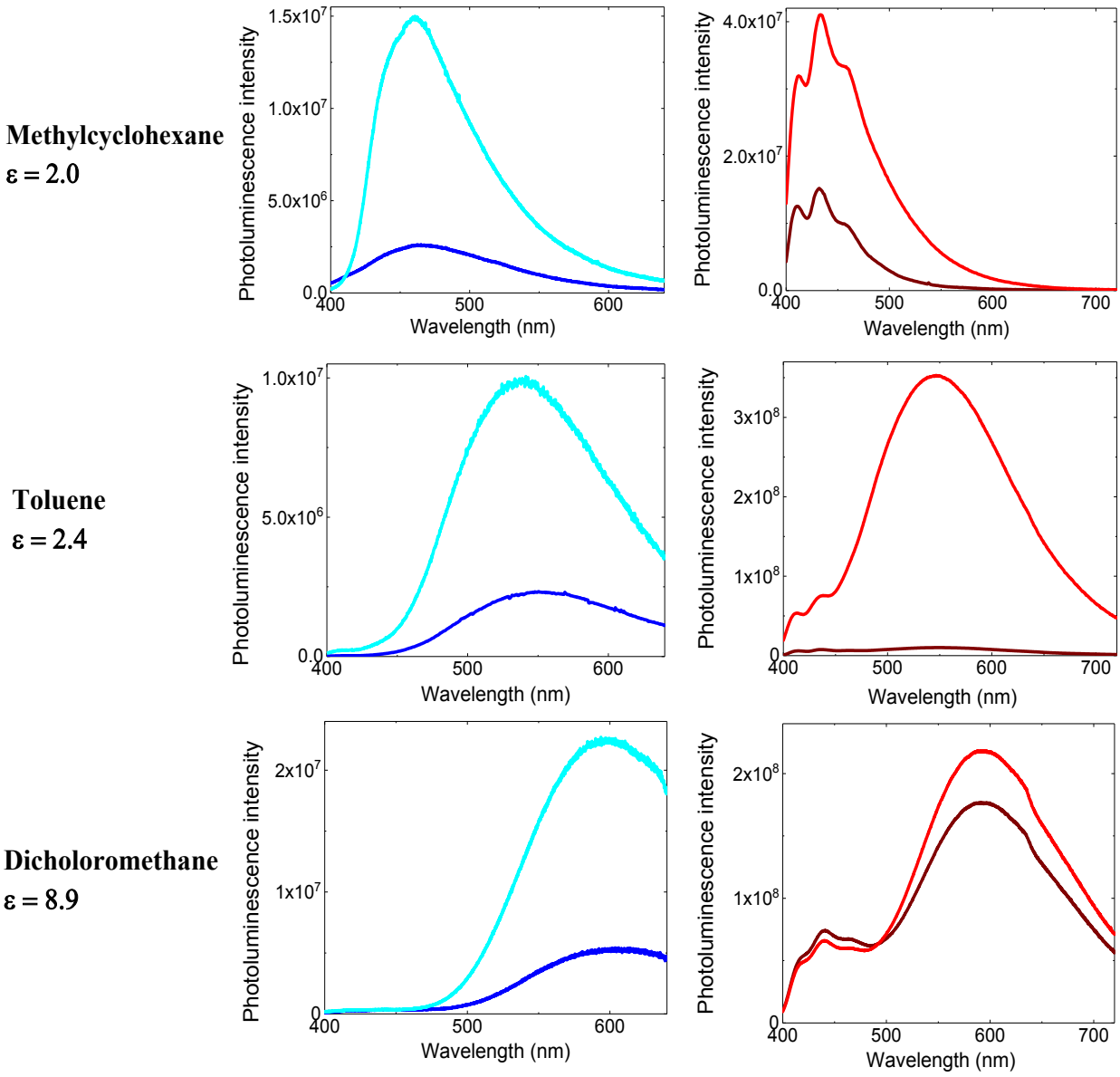


**Supporting Figure S9.** Comparison of the effect of solvent on the emission of ACRSA dissolved in solvents of different polarity at concentration 1 mg/mL. (Left: Emission spectra measured at $\lambda_{exc} =$ 330 nm, with oxygenated spectra in dark blue and deoxygenated spectra in light blue. Right: Emission spectra measured at $\lambda_{exc} =$ 380 nm, where oxygenated spectra is in maroon and deoxygenated spectra in red). Emission intensity is given in absolute counts.

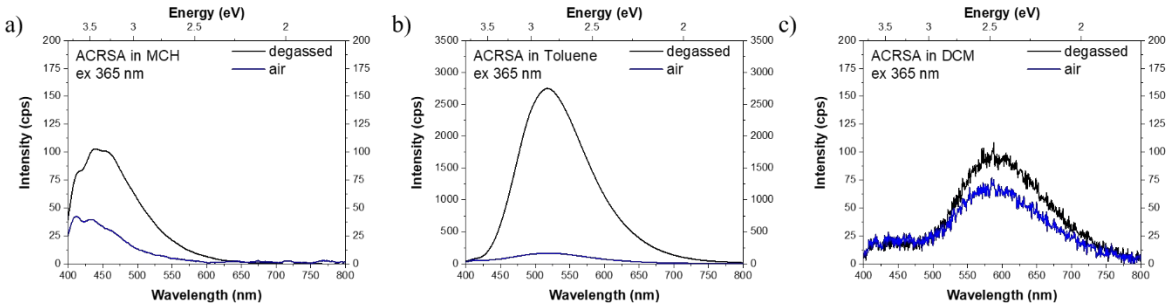


**Supporting Figure S10.** Solution state emission spectra (aerated and degassed) for ACRSA dissolved in MCH (a), Toluene (b) and DCM (c) (50 μM). Excitation 365 nm, showing much greater DF contribution in toluene than in MCH and DCM.

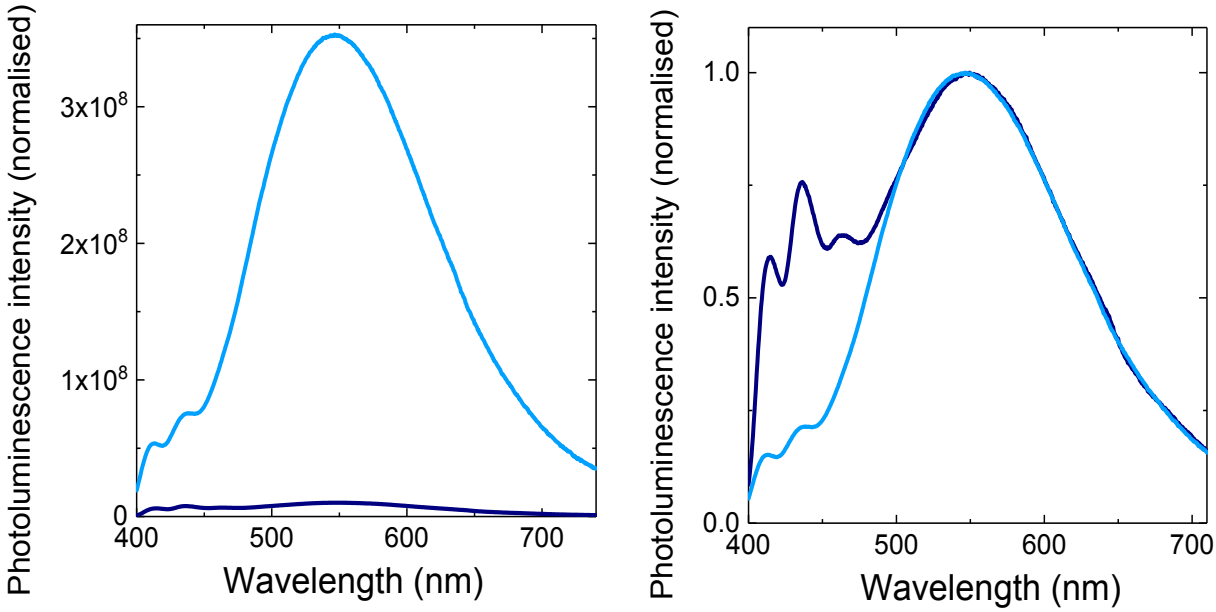


**Supporting Figure S11.** Absolute (left) and normalised (right) emission spectra of ACRSA dissolved in toluene solution (1 mg/mL) measured at $\lambda_{exc} =$ 380 nm, with oxygenated spectra shown in dark blue and deoxygenated spectra in light blue. The large increase in absolute emission intensity on degassing comes purely from delayed CT emission.

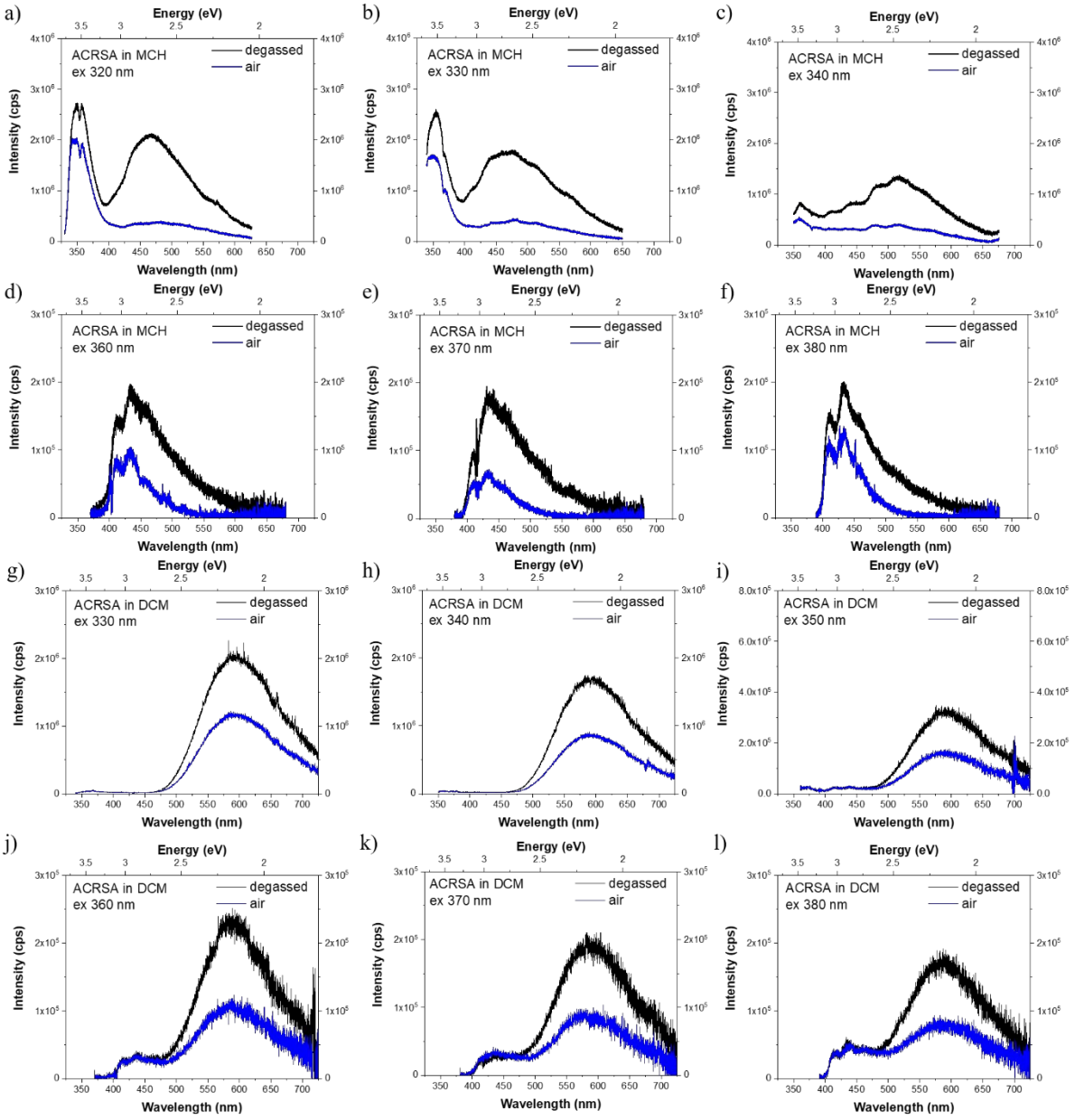


**Supporting Figure S12.** Solution state emission spectra (aerated and degassed) for ACRSA in MCH (a-f) and DCM (g-l) (50 μM) measured at six different excitation wavelengths; 330 nm to 380 nm (non-normalised data). Top rows (a-c and g-i) are spectra with the excitation wavelength exciting the $1^1B_1$ exciton transition, bottom rows (d-f and j-l) with excitation into the $2^1A_2$ and $1^1A_2$ transitions. In MCH, three states emit simultaneously, completely at odds with Kasha's Law, whereas in DCM the high energy emission band is quenched.

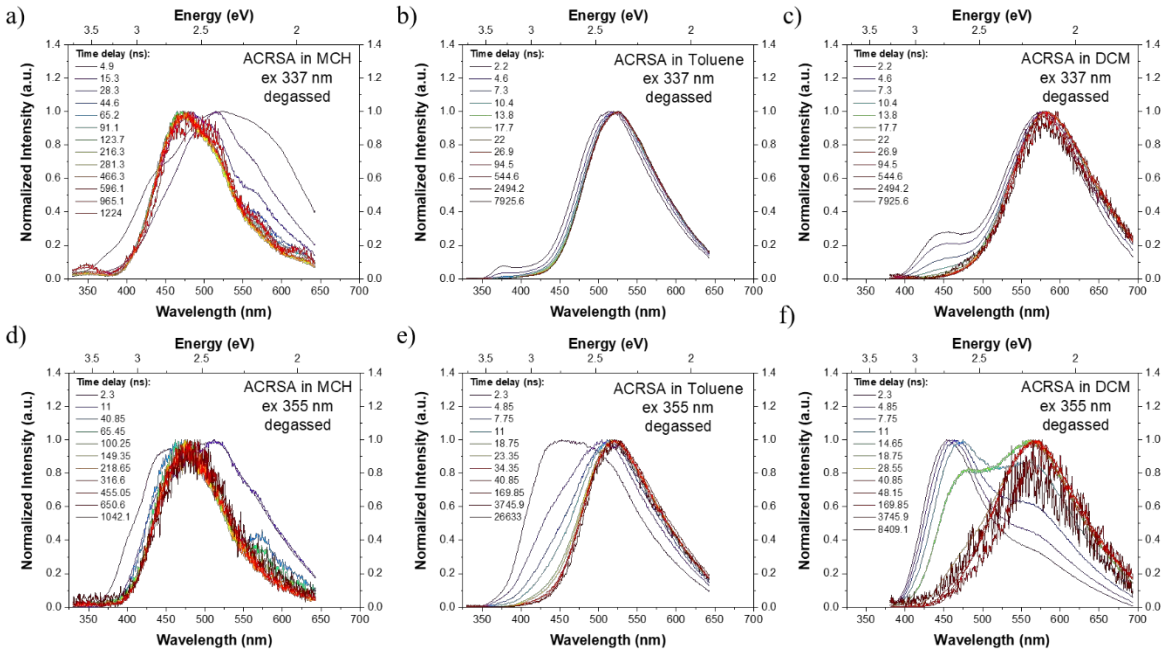


**Supporting Figure S13.** Peak normalised time resolved emission decay of ACRSA in MCH, toluene and DCM solutions (concentration 50 µM) excited at 337 nm into the $1^1B_1$ exciton transition (a-c) and at 355 nm into the direct mixed $2^1A_2$ and $1^1A_2$ transitions (d-f).

**a)**

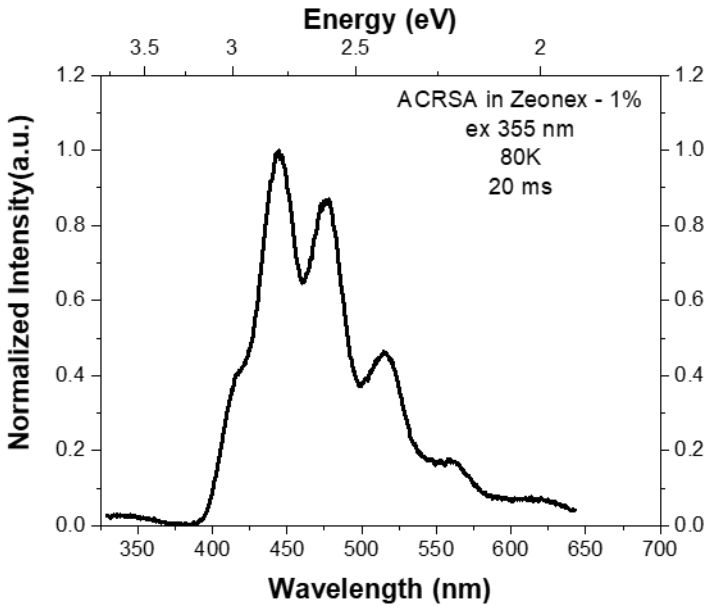


**b)**

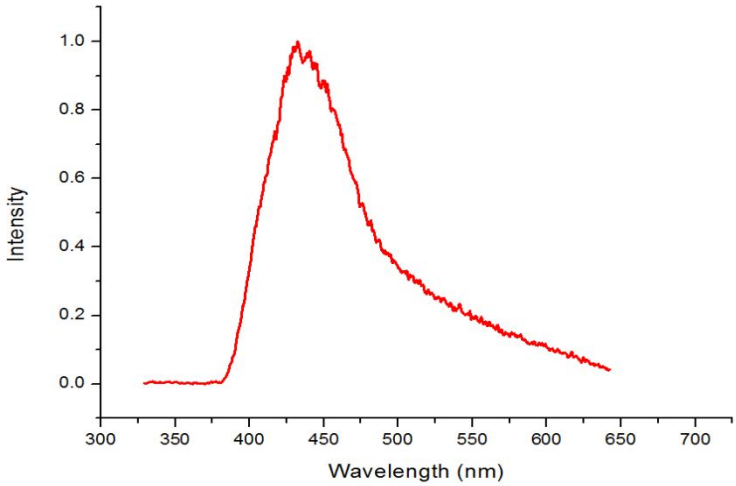


**Supporting Figure S14.** Low temperature phosphorescence spectra of ACRSA in Zeonex matrix (1%wt) obtained by time-resolved PL, a) at 80 K and 20 ms delay, b) 80 ms delay.

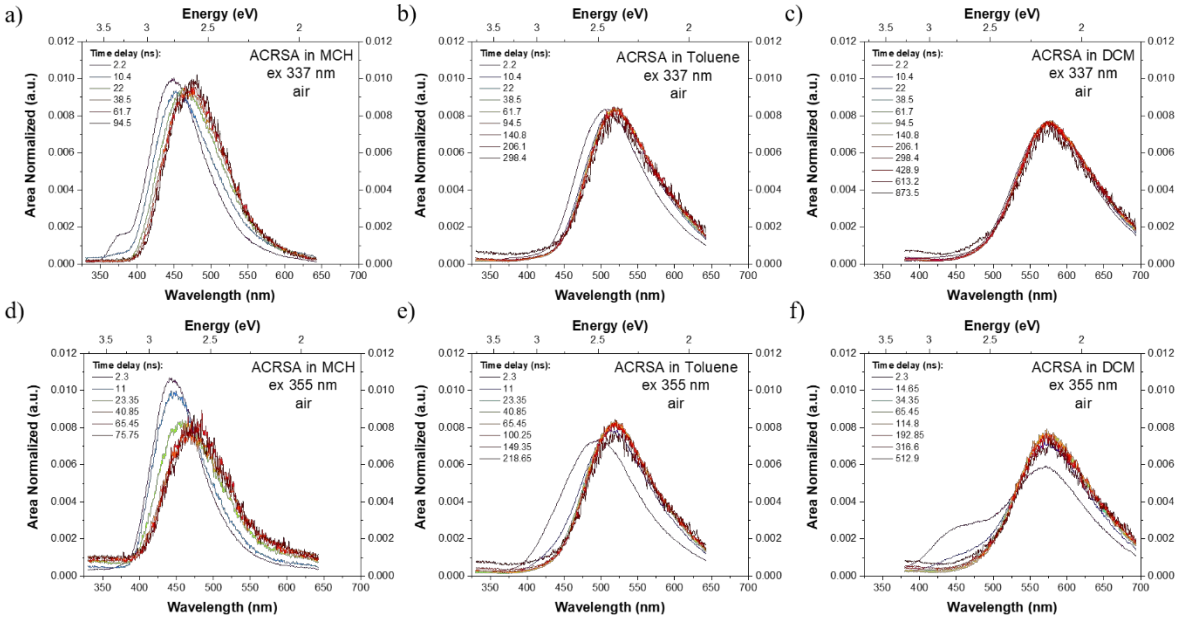


**Supporting Figure S15.** Area normalised time resolved emission decay of ACRSA in aerated MCH, toluene and DCM solutions (concentration 50 µM) excited at 337 nm into the $1^1B_1$ exciton transition (a-c) and at 355 nm into the direct mixed $2^1A_2$ and $1^1A_2$ transitions (d-f).

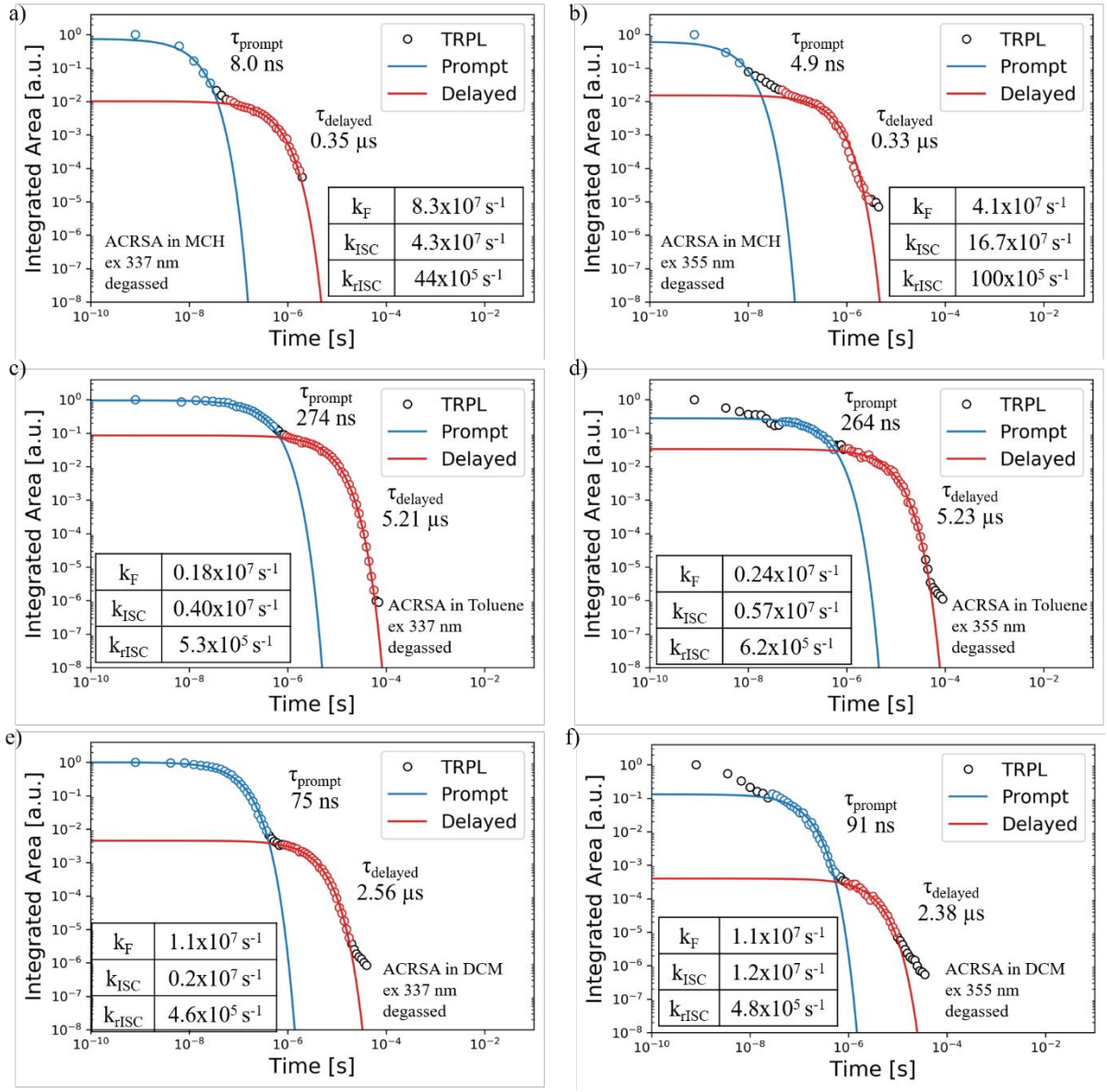


**Supporting Figure S16.** Time-Resolved PL decays of ACRSA in degassed MCH, toluene and DCM solutions (concentration 50 µM) excited at 337 nm into the $1^1B_1$ exciton transition (a, c, e) and at 355 nm into the direct mixed $2^1A_2$ and $1^1A_2$ transitions (b, d, f). The data is fitted using a kinetic model described by Haase et al.[3]

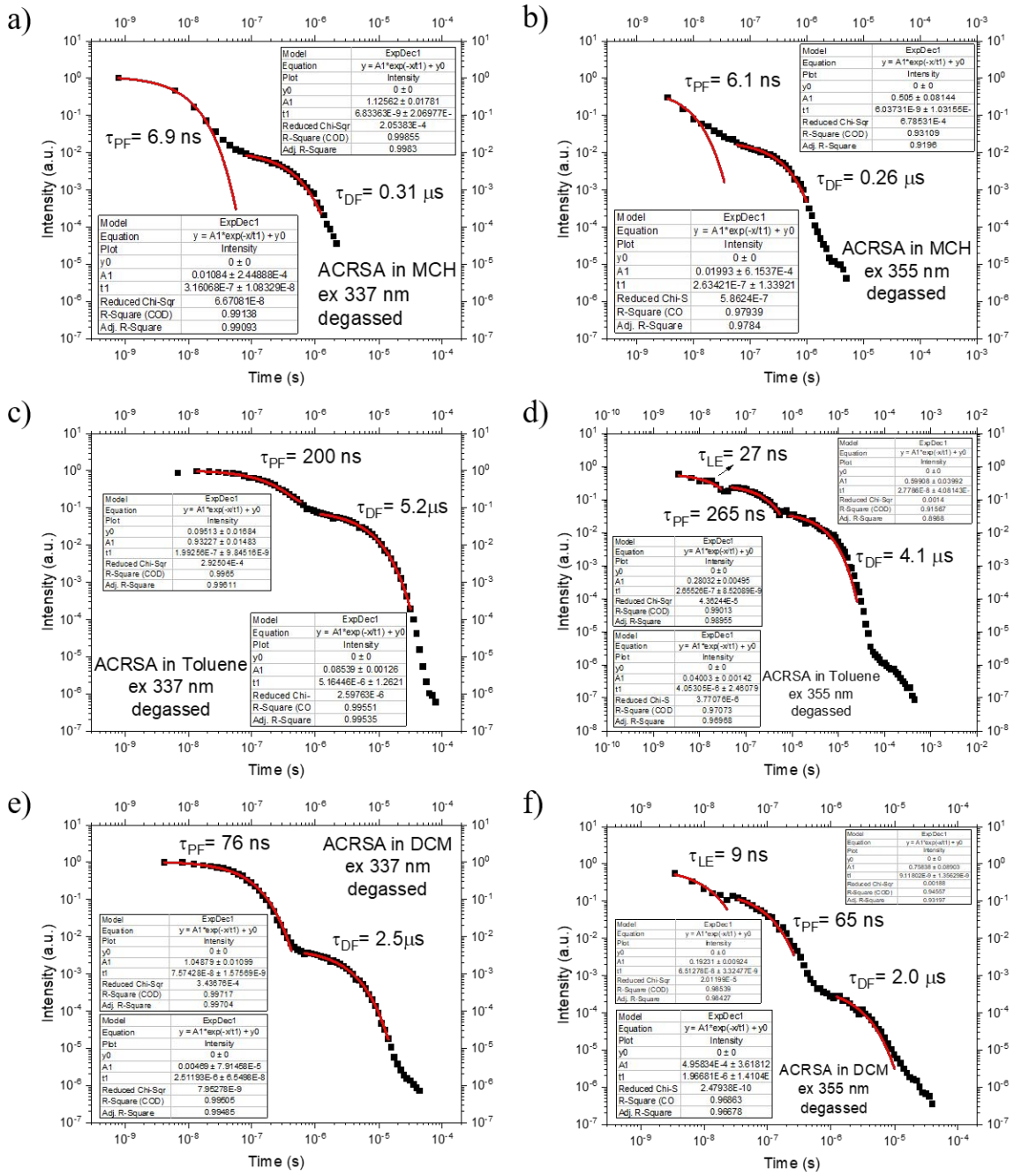


**Supporting Figure S17.** Time-Resolved PL decays of ACRSA in degassed MCH, toluene and DCM solutions (concentration 50 µM) excited at 337 nm into the $1^1B_1$ exciton transition and at 355 nm into the direct mixed $2^1A_2$ and $1^1A_2$ transitions. The data is fitted using a mono exponential function, in order to compare with the fitting obtained in Supporting Figure S16.

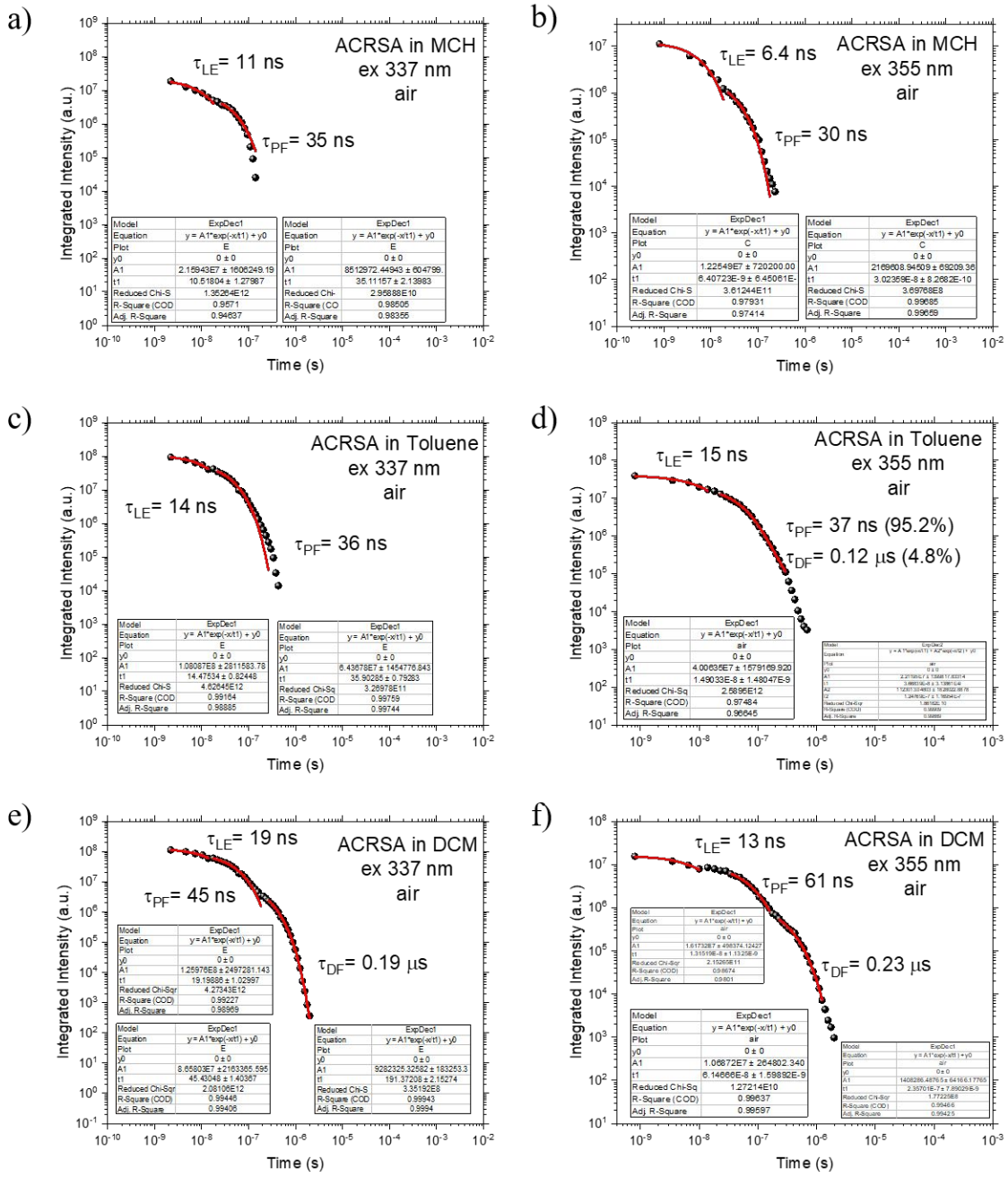


**Supporting Figure S18.** Time-Resolved PL decays of ACRSA in aerated MCH, toluene and DCM solutions (concentration 50 μM) excited at 337 nm into the $1^1B_1$ exciton transition and at 355 nm into the direct mixed $2^1A_2$ and $1^1A_2$ transitions. The data is fitted using a mono and bi exponential function.

**Table 1.** Kinetic model results for ACRSA in different solvents with 355 nm excitation.

| | **Prompt LE (ns)** | **Prompt CT (ns)** | **Delayed CT (µs)** | **$k_{rad}$ ($x10^7$ $s^{-1}$)** | **$k_{ISC}$ ($x10^7$ $s^{-1}$)** | **$k_{rISC}$ ($x10^5$ $s^{-1}$)** |
|---|---|---|---|---|---|---|
| **337 nm excitation (degassed)** | | | | | | |
| **MCH** | ~2** | 8±3 | 0.35±5 | 8.3 | 4.3 | 44 |
| **Toluene** | ~2** | 274±5 | 5.21±0.02 | 0.176 | 0.399 | 5.29 |
| **DCM** | ~10** | 75±1 | 2.56±0.02 | 1.10 | 0.175 | 4.56 |
| **337 nm excitation (aerated) *** | | | | | | |
| **MCH** | 11±2 | 35±2 | - | | | |
| **Toluene** | 14±1 | 36±1 | - | | | |
| **DCM** | 19±1 | 45±2 | 0.19±0.03 | | | |
| **355 nm excitation (degassed)** | | | | | | |
| **MCH** | ~2** | 4.9±0.2 | 0.33±10 | 4.06 | 6.7 | 100 |
| **Toluene** | - | 264±5 | 5.23±0.06 | 0.24 | 0.57 | 6.2 |
| **DCM** | 9±3* | 91±3 | 2.38±0.06 | 1.12 | 0.118 | 4.83 |
| **355 nm excitation (aerated) *** | | | | | | |
| **MCH** | 6.4±0.7 | 30.2±0.9 | - | | | |
| **Toluene** | 15±2 | 37±3 | 0.12±0.02† | | | |
| **DCM** | 13±1 | 61±2 | 0.236±0.01† | | | |

* Value obtained by exponential fitting (Supporting Figure S17 and S18).
** Value estimated by time resolved photoluminescence spectra.
† Less than 5% of emission.

## References


(1) Lyskov, I.; Marian, C. M. Climbing up the Ladder: Intermediate Triplet States Promote the Reverse Intersystem Crossing in the Efficient TADF Emitter ACRSA. *J. Phys. Chem. C* **2017**, *121*, 21145–21153.

(2) dos Santos, P. L.; Ward, J. S.; Bryce, M. R.; Monkman, A. P. Using Guest–Host Interactions To Optimize the Efficiency of TADF OLEDs. *J. Phys. Chem. Lett.* **2016**, *7*, 3341–3346.

(3) Haase, N.; Danos, A.; Pflumm, C.; Morherr, A.; Stachelek, P.; Mekic, A.; Brütting, W.; Monkman, A. P. Kinetic Modeling of Transient Photoluminescence from Thermally Activated Delayed Fluorescence. *J. Phys. Chem. C* **2018**, *122*, 29173–29179.